Journal of Molecular Graphics and Modelling 49 (2014) 25–37

Contents lists available at ScienceDirect

Journal of Molecular Graphics and Modelling

journal homepage: www.elsevier.com/locate/JMGM

# Discovery of potent inhibitor for matrix metalloproteinase-9 by pharmacophore based modeling and dynamics simulation studies

Sukesh Kalva [a], E.R. Azhagiya Singam [b], V. Rajapandian [b], Lilly M. Saleena [a], V. Subramanian [b,*]

[a] Department of Bioinformatics, SRM University, Kattankulathur, Kancheepuram District 603 203, India
[b] Chemical Laboratory, Central Leather Research Institute, Council of Scientific and Industrial Research, Adyar, Chennai 600 020, India

ARTICLE INFO

*Article history:*
Accepted 20 December 2013
Available online 2 January 2014

*Keywords:*
Pharmacophore modeling
Docking
Molecular dynamics simulation
MTT
Gelatin zymography

ABSTRACT

Matrix metalloproteinase-9 (MMP-9) is an attractive target for anticancer therapy. In the present study ligand based pharmacophore modeling was performed to elucidate the structural elements for a diverse class of MMP-9 inhibitors. The pharmacophore model was validated through Güner-Henry (GH) scoring method. The final pharmacophore model consisted of three hydrogen bond acceptors (HBA), and two ring aromatic regions (RA). This model was utilized to screen the natural compound database to seek novel compounds as MMP-9 inhibitors. The identified hits were validated using molecular docking and molecular dynamics simulation studies. Finally, one compound named Hinokiflavone from Juniperus communis had high binding free energy of −26.54 kJ/mol compared with the known inhibitors of MMP-9. Cytotoxicity for hinokiflavone was evaluated by MTT assay. Inhibition of MMP-9 in the presence of hinokiflavone was detected by gelatin zymography and gelatinolytic inhibition assay. Results revealed that the natural compounds derived based on the developed pharmacophore model would be useful for further design and development of MMP-9 inhibitors.



## 1. Introduction

Matrix metalloproteinases (MMPs) are the family of zinc-dependent neutral endopeptidases that are collectively capable of degrading essentially all the components of the extracellular matrix [1–4]. They are classified as collagenases, gelatinases, stromelysins and matrilysin according to their substrate specificity [5,6]. They constitute the main group of proteolytic enzymes that are involved in the tumor invasion, metastasis, and angiogenesis [7,8]. Among all, matrix metalloproteinase-9 (MMP-9) is particularly involved in inflammatory processes, bone remodeling and wound healing. It is also implicated in pathological processes such as rheumatoid arthritis, atherosclerosis, tumor growth, and metastasis [9–11]. Difference in production levels of regulatory mechanisms of MMP-9 subsequently results in restricted, extensive, or improperly timed degradation of extracellular matrices [12]. The role of MMP-9 in many pathological diseases has laid a foundation for the identification of selective inhibitors.

The structure of the MMPs includes a signal peptide, a propeptide, a catalytic domain with a highly conserved zinc-binding site, and a haemopexin-like domain, which is linked by a hinge region [13]. The structure of the catalytic domain of human MMP-9 (without the fibronectin repeats) consists of five-stranded β-sheet and three α-helices, which is similar to other MMPs. The catalytic center is composed of the active-site zinc ion, which is co-ordinated by three histidine residues (401, 405 and 411) and an essential water molecule [14]. MMP-9 is illustrious among the other MMPs by the incidence of three head to tail cysteine rich repeats which resemble fibronectin type II repeats. This insert is mandatory for their interaction with substrates like gelatin, laminin and collagen [15]. In most of the MMPs, the hydrophobic specificity (S1) pocket is the major determinant for their substrate specificity [16]. The specificity loop greatly differs in length among MMPs and encompasses from nine (in MMP-1, -9, -11, and -23) to 13 residues (in MMP-17 and -25) [17]. In MMP-1 and MMP-7, the size of the S1 subsite is reduced by the presence of arginine and tyrosine respectively. In other MMPs, the S1 cavity has a long open channel with different amino acid residues [18]. For example in MMP-2, the S1 loop is mainly delimited by the presence of Pro417, Gly418, Ala422, Ile424, and Thr426, and showed a large aperture at the end of the pocket [16]. In contrast to MMP-2, the S1 pocket of MMP-3 is delimited by different residues (Thr232, Glu233, Tyr237, Leu239, and His241) and exhibits a smaller aperture at the end of the cavity. Another interesting difference is the role played by specific S1 loop residues which can influence the access of a long side chain residue of the substrate into the S1 cavity of MMPs [18].

* Corresponding authors. Tel.: +91 44 24411630; fax: +91 44 24911589.
*E-mail addresses:* saleena.m@ktr.srmuniv.ac.in (L.M. Saleena), subuchem@hotmail.com, subbu@clri.res.in (V. Subramanian).

1093-3263/$ – see front matter © 2013 Elsevier Inc. All rights reserved.
http://dx.doi.org/10.1016/j.jmgm.2013.12.008

Most MMPs inhibitors are classified according to their ZBG. The most common ZBG used in MMPI is the hydroxamic acid group which tightly binds with the catalytic zinc ion using two identical bonds and extends the binding in the P1 and S1′ selectivity pockets of MMPs. These hydroxamic acid inhibitors produced nanomolar inhibitors with high potency against MMPs. The failure of hydroxamic acid in the clinical trials is due to lack of selectivity toward zinc ion and poor pharmacokinetics and oral bioavailability. A number of efforts have been made to identify alternatives to the hydroxamic acid group. Later hydroxamic acid group was replaced by the carboxylic acid groups which results loss in potency. This is due to the changes in binding mode of carboxylate ligand in the active site of MMPs. However, Castelhano and co-workers reported the selectivity and potency of MMPI with several different ZBGs (for example, hydroxamates, 'reverse' hydroxamates, carboxylates, thiols, phosphinates) on a common indolactam/isobutyl backbone moiety. In contrast, the unique findings reported strongly that high affinity ZBGs can be used as the basis for new patterns of selective inhibition against MMPs. This indicates that by linking the different zinc binding groups with the common backbone can improve the selectivity against deep S1′ pocket of MMPs [19].

Several generations of synthetic MMP inhibitors (MMPIs) have been tested in phase III trials on humans such as hydroxamate, non hydroxamate, synthetic collagen peptido-mimetic, non-peptidic, synthetic tetracycline derivatives and biphosphonate inhibitors, and have been demonstrated to have no therapeutic efficacy [20]. Several grounds for the failure of MMPIs in human clinical studies include high toxicity, which causes severe musculoskeletal side-effects and the lack of specificity of the inhibitors, which can lead to unexpected and redundant effects [21,22]. Regardless of the clinical failures, the recent development of highly selective inhibitors for MMP-12 and MMP-13 suggests that specific targeting of metzincins may not be difficult [23,24]. The negative results obtained from the clinical trials for the synthetic compounds stirred up an interest to work on the natural compounds. There are prior reports on the inhibitory activity of natural compounds against MMPs [25]. For example myricetin, a flavonoid found in berries, fruits, vegetables, herbs and tea greatly decreased the activity of MMP-2 in human colorectal carcinoma cell lines. Neovastat (shark cartilage) was analyzed in regard to anti-angiogenic and anti-metastatic effects on the activity of several MMPs. Neovastat inhibits the enzymatic activity of MMP-2 with minor inhibition of MMP-1, 9, 7 and 13 [26]. Hence natural compounds could be a better choice for selective inhibition of MMP-9.

In modern computational biology, pharmacophores based approach is used to delineate the essential features of one or more molecules with the same biological activity. The pharmacophore based modeling of ligands is a well-established approach to quantitatively discover common chemical features among a considerable number of structures. Pharmacophore mapping can be used in designing the inhibitors in several ways, including justification of activity trends in molecules, searching of databases to find new chemical entities and to identify important features for activity [27].

In this study, the pharmacophoric features of the inhibitors of MMP-9 have been developed. The pharmacophore based modeling has been carried out to identify the best features, such as hydrogen bond acceptor, donor, aromatic ring, and aliphatic chain for MMP-9, from the existing drug which facilitates the drug activity for the identification of novel inhibitors from the natural compound database. Furthermore, docking and molecular dynamics (MD) simulation were performed to analyze the binding affinity of the identified natural compounds. The high scored hit from MD studies was taken for in vitro studies to check the biological activity against MMP-9. The overall workflow for ligand-based pharmacophore in screening the novel compounds for MMP-9 is given in Fig. 1.

## 2. Materials and methods

### 2.1. Ligand preparation

A data set of ligand molecules having MMP-9 inhibitory activity were collected from the literature (Supporting information Table S1) [28–36]. Quantitative pharmacophore was generated for the molecules based on the diversity of their chemical structure and biological activity against human MMP-9 inhibitors. The MMP-9 inhibitors used in this study were further energy minimized using Ligprep module of Schrödinger software [37]. The conformations of the above structures were generated using the MMFFs force field, with an implicit GB/SA solvent model. A maximum of 1000 conformers were generated per structure by a preprocess minimization of 1000 steps using ConfGen algorithm. During the search, hydrogen-bonding interactions were suppressed to facilitate conformations in which the ligand bonds to the receptor, and not just conformations with internal hydrogen bonding, as this is essential for the model.

### 2.2. Pharmacophore model generation

The quantitative pharmacophore model was built using the Phase software [38]. The diverse dataset were used to generate

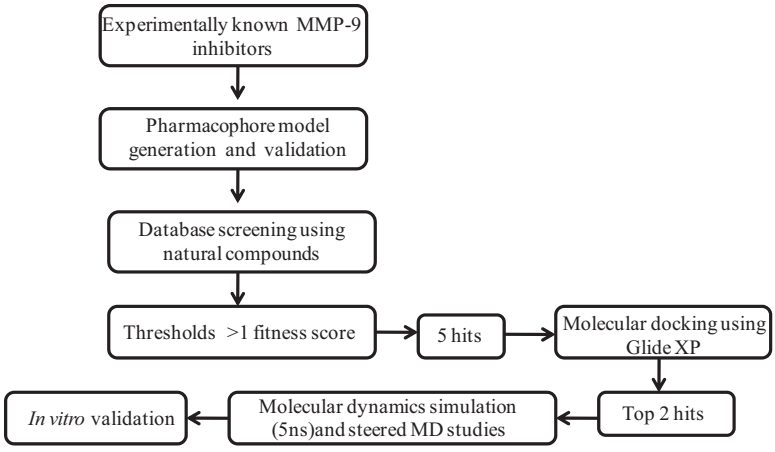


**Fig. 1.** Workflow for identifying novel inhibitors using ligand-based pharmacophore modeling.

the pharmacophore model. Ligands with $pIC_{50}$ value ranging from 5.42 to 9.00 were taken for generating the pharmacophore model. Active and inactive threshold of $pIC_{50}$ of 8.00 and 5.42 were applied for the dataset to yield 24 actives, 14 inactive and 51 moderately actives. 24 highly active compounds i.e. compounds with the activity greater than 8.00 were used for pharmacophore model generation. For actives, the compounds used had hydroxamic acid as zinc binding group with different groups substituted at 4-arylsulfonylpiperidine. For inactives, the carboxylates as zinc binding groups with different substitutions like alkynyloxy phenyl sulfanyl, sulfinyl, and sulfonyl alkyl, were used. A set of pharmacophore features for the MMP-9 inhibitors were produced using create sites option, which creates the site points for each conformer of the above ligands. A default setting having acceptor (A), donor (D), hydrophobic (H), negative (N), positive (P), and aromatic ring (R) features were used to create pharmacophore sites. Pharmacophore hypotheses common for the set of active ligands were generated using these pharmacophore features. Common pharmacophores are identified from a set of variants, which is a set of feature type that defines a possible pharmacophore using a tree based portioning algorithm. The common pharmacophore hypotheses from the active ligands were scored by setting the root mean square deviation (RMSD) value below 1.0, the vector score value to 0.5. Higher survival score resembles better mapping of the pharmacophore with the active molecules. Apart from the survival score, fitness score was also used to confirm the quality of pharmacophore hypothesis [39].

### 2.3. Pharmacophore model validation

The pharmacophore model selected was then validated by Güner-Henry (GH) scoring method. This method quantifies the hits by recalling the actives from inactives from the database containing 2548 molecules. Of these 2548 molecules, 48 molecules are known inhibitors of MMP-9 with diverse activities. While the other 2500 are decoy molecules downloaded from the DUD decoys database (http://dude.docking.org/targets/mmp13). The same active groups cannot be used since the decoys were not available in DUDE database. So, the MMP-13 decoys were used in the 1:50 ratio to find the enrichment of the developed pharmacophore model. This database with known actives and inactives was screened with the ligand and protein based pharmacophore models to calculate the GH score. The GH score has been successfully applied to quantify model selectivity, accuracy of hits and the recall of actives from a molecule dataset consisting of known actives and inactives. The GH score ranges from 0, which indicates the null model, to 1, which indicates the ideal model. Formulae to analyze the hit lists by a ligand based pharmacophore models based database search [40–42].

$$\%A = \frac{Ha}{A} \times 100 \quad (1)$$

$$\%Y = \frac{Ha}{Ht} \times 100 \quad (2)$$

$$E = \frac{Ha/Ht}{A/D} \quad (3)$$

$$GH = \left(\frac{Ha(3A + Ht)}{4HtA}\right)\left(1 - \frac{Ht - Ha}{D - A}\right) \quad (4)$$

where $\%A$ is the percentage of known active compounds obtained from the database, $Ha$ is the number of actives in the hits list (true positives), $A$ is the number of active compounds in the database, $\%Y$ is the percentage of known actives in the hits list (recall), Ht is the number of hits retrieved, $D$ is the number of compounds in the database, $E$ is the enrichment of the concentration of actives by the model relative to random screening without a pharmacophoric approach, and GH is the Güner-Henry score. GH score of 0.6–1 indicates a very good model.

### 2.4. Database screening

The developed Pharmacophore hypothesis was further screened for the Duke's database of natural compounds holding 400 molecules with biological activities like anticancer, antioxidant, anti inflammatory, antifungal and antimicrobial to screen for potent inhibitor for MMP-9. The criteria for finding out the hits was that all the five out of five pharmacophoric features must match with default inter feature distance. Duke's database was scanned for geometric arrangements of pharmacophore sites that match the above generated hypothesis within a tolerance applied to the inter site distances. Molecules with fitness score above 1 were taken for docking studies. The list of 400 compounds along with their PubChem ID and name was given in Supporting Information (as excel sheet).

### 2.5. Glide ligand docking

Glide module was used to perform docking of the ligands to MMP-9 [43]. Among 14 crystal structures, the PDB ID: 1GKC was chosen, because it is the first reported structure for MMP-9 bound to a reverse hydroxamate inhibitor. The reverse hydroxamate inhibitors have better pharmacokinetic properties than their hydroxamate counterparts and therefore may present a more useful starting point for drug design. Protein was prepared using protein preparation wizard which assigns bond order and adds hydrogen. The active site of the protein was defined using default parameters of receptor grid generation. Ligands were energy minimized using the Ligprep module. Docking was performed using XP docking mode (Extra Precision). The results of the docking were then quantified in terms of the Glide score and Glide energy.

### 2.6. Molecular dynamics (MD) simulation of MMP-9–ligand complex

#### 2.6.1. Calculation of partial charges

Catalytic Zn ion is modeled as a tetrahedral geometry coordinated by the three HIS from the conserved motif and a water molecule. The structural Zn ion is modeled as a tetrahedral geometry coordinated by three His and one Asp residue. The truncated active sites of MMP-9 were used to derive the force field. The hydrogen atoms were added to the models, and their positions were optimized at the B3LYP/6-31G(d,p) level by freezing coordinates of heavy atoms. The PES scans were performed using the DFT (B3LYP) method employing the 6-31G(d,p) basis set to predict the stretching and bending force constants for the truncated active site models of MMP-9 active site. The PES scans were carried out by a systematic variation of the M(II)–L distances and ligand–metal ion–ligand [L–M(II)–L] angles by fixing all other coordinates with the distance interval and number of steps are 0.001 Å and 11, respectively. For angle, distance interval and number of steps is 0.1° and 11, respectively. All calculations were carried out using Gaussian 03 (Revision E.01) package [44]. The potential energy barriers for the dihedral angles centered on a metal ion are usually considered to be of minor importance for the dynamics and energetics of metalloproteinase [45–48]. Therefore, all force constants for dihedral angles with a metal ion as the second or third atom were set to zero. Atomic charges for the metal ions and all of the other atoms in the cluster models were calculated using the B3LYP/6-31G(d,p) level of theory (Supporting information S2) [49–55]. The van der Waals (R) parameter for Zinc was taken as 1.10 Å and $\varepsilon$ was taken as 0.0125 kcal/mol. The restrained electrostatic potential (RESP)

charges were generated by the standard method prescribed in the AMBER package [56]. Calculated bond distances, bond angles, and corresponding force constants are given in Supporting information Table S3.

*2.6.2. Molecular dynamics (MD) simulation*

MD simulations of all the systems were carried out using GROMACS 4.5.3 package [57]. The MMP-9 ligand complex obtained from docking was solvated with TIP3P water. Calculations were carried out by employing AMBER FF99SB force field. The solvated system was subjected to 500 steps of energy minimization employing the steepest descent algorithm. This step was followed by 250 pico second (ps) MD simulation, where the MMP-9–ligand complex was position restrained to equilibrate the water and ions under the influence of solute. The production run was carried out for all the systems for 5 nano seconds (ns) using 1 femto second (fs) time step for the integration of equation of motion in the NPT ensemble at 300 K and at 1 atmospheric pressure, which were controlled by V-rescale thermostat and Parrinello-Rahman Barostat, respectively. Bond length involving hydrogen atoms were constrained by using LINCS algorithm [58]. The Particle-Mesh Ewald (PME) was used to calculate the electrostatic interaction with the cutoff of 10 Å. The MD simulation coordinates of all the systems were saved at 1 ps interval for further analyses. Post processing and analyses were carried out using GROMACS analysis tools. Visual Molecular Dynamics (http://www.ks.uiuc.edu/Research/vmd/) and PyMol packages were used for visualization analysis.

*2.6.3. Steered molecular dynamics simulation*

Steered molecular dynamics (SMD) simulation was carried to understand the force required to pull out the ligand from the protein [59]. Input configurations for the SMD simulations were generated from the final geometry of the MD simulation. Each Model was solvated in the box with the dimension of $60 \times 60 \times 90$ Å. The systems were again equilibrated for 250 ps. Pulling of ligand was performed by the SMD simulation method. This method is based on the concept of pulling the center of mass of a collection of chosen atoms via a spring along the $z$ direction, while keeping the center of mass of protein atoms fixed through a spring constant. The center of mass of protein atoms was fixed with the constant of $1 \times 10^5$ kJ mol$^{-1}$ nm$^{-2}$, and the center of mass of ligand was linked to a spring with an elastic constant $k_{spring} = 500$ kJ mol$^{-1}$ nm$^{-2}$ which was pulled along the direction of molecular axis with the pulling velocity of 0.005 m/s.

## 3. Experimental assays

### 3.1. Cell culture preparation

The human breast cancer MCF-7 cell line was cultured in Dulbecco's modified Eagle's medium (DMEM) trypsinized and complemented with 10% fetal calf serum (FCS). MCF-7 cells were cultured at 37 °C in a 5% $CO_2$ incubator.

### 3.2. MTT assay

The cells were seeded in 96-well microtitre plate (100 μl/well) with a concentration of $4 \times 104$ cells/cm$^2$ [60–62]. At 80% confluency, the cultivated cells were exposed to various concentration of the compound (25, 50, 100, 200, 300, 400, 500, and 600 μg/mL) prepared in 1% dimethyl sulfoxide (DMSO) and were incubated for 48 h. Control groups received the same amounts of DMSO with four wells remained untreated as control. After the treatment, normal culture medium was substituted with 200 μl fresh media and 50 μl MTT reagent (2 mg/mL in PBS), except the cell-free blank control wells. Cells were maintained in 37 °C with 5% $CO_2$ and complete humidity for 4 h. Subsequently, the MTT solution was replaced with 100 μl of DMSO incubated for 15 min at 37 °C. Later, the optical density (OD) of the wells was measured at 570 nm by means of a spectrophotometric plate reader (Bio Rad, USA). The viability of the cells was determined using the formula:

$$\text{viability\%} = \frac{\text{OD of sample}}{\text{OD of control}} \times 100 \quad (5)$$

The $LC_{50}$ of the compound was determined by plotting cell viability against respective concentration of the compound.

### 3.3. Gel zymography

MCF-7 cell supernatant was subjected to zymography assay for qualitative estimation of MMP9 activity. The total protein content of the supernatant was 1 μg/μl (Lowry method) and 20 μl was added to zymogram gel [63]. Zymogram gel constituted 8% polyacrylamide gel and 1 mg/mL of gelatin was polymerized and was used for zymography procedure [64]. The gel was electrophoresed at 125 V and subsequently washed with wash buffer (2.5% Triton X 100). After 20 hours of incubation at 37 °C in a solution of 0.15 M NaCl, 10 mM $CaCl_2{\cdot}2H_2O$, 50 mM Tris–HCl, 0.5 g $NaNO_3$, The gel was stained with CBB G-250 for an hour and destained with 10% methanol, 2% acetic acid. Clear regions of gelatinolytic activity were observed using alpha-view software.

### 3.4. Gelatinolytic enzyme assay for estimation of $IC_{50}$

Colorimetric gelatinolytic assay with Coomassie Brilliant Blue (CBB R-250) is used to measure bacterial collagenase type II inhibition study [65]. Here, the protocol and the buffer composition have been modified for optimal performance of gelatinase class of MMP-9 activity and its quantitative estimation of enzyme inhibition. The action of CBB R-250 on gelatin forms a complex, which precipitates out of solution. The blue pellet was dissolved in suitable solvent viz., Dimethyl sulfoxide ($Me_2SO$) and the absorbance were read at 600 nm. The CBB R-250 was dissolved, filtered through Whatman 80, No-1 and heated in microwave at high power for 3 minutes (0.125%, w/v, CBB R-250 in 40% methanol and 10% acetic acid). The standard plot for the gelatin substrate (0.1–10 μg in PBS) was quantified in a total volume of 10 μl with 400 μl of the staining dye. After incubation at 37 °C for 5 min, the precipitate was centrifuged at $8000 \times g$. The pellet was dissolved in 1000 μl $Me_2SO$ followed by determination of $R^2$ correlation coefficient at absorbance 600 nm ($A_{600}$). MMP-9 from the MCF-7 cell supernatant was purified using gelatin–sepharose chromatography as per Morodomi et al. [66]. The presence of MMP-9 in the eluted sample was confirmed with SDS-PAGE which was taken as control for all the inhibitory studies. The enzyme assay was performed by incubating 20 μl of the MMP-9 (E0) with 10 μl of 10 μg gelatin substrate at 37 °C for 4 h. The quantity of the gelatin degraded was determined as described above. The inhibitory effect of hinokiflavone on MMP-9 was studied by varying the concentrations of inhibitor from 10 μM to 250 μM in PBS. Equal volumes of these varying concentrations were incubated with the enzyme (total volume 40 μl) for 1 h at 37 °C. Thereafter, this enzyme-inhibitor (EI) sample was incubated with 10 μl of 10 μg gelatin substrate at 37 °C for 4 h. The amount of gelatin degraded was estimated as described above. All the enzyme assays were performed along with a blank (B), substrate blank (SB) and enzyme blank (EB). The control enzyme assay and the inhibition assays were performed simultaneously to obtain justifiable results.

**Table 1**
The best 3 common pharmacophore hypotheses with survival active scores.

| Hypothesis | Survival active |
|---|---|
| AAARR.1813 | 3.707 |
| AADRR.667 | 3.702 |
| AAARR.133 | 3.694 |

### 3.5. Binding free energy analysis

The binding affinities of both ligands with MMP-9 were calculated using following Eq. (1):

$$\Delta G_{binding} = \alpha(\langle E\_VdW_{bound}\rangle - \langle E\_VdW_{,free}\rangle) + \beta(\langle E\_Coul_{bound}\rangle - \langle E\_Coul_{,free}\rangle) \quad (6)$$

where $E\_VdW_{bound}$ and $E\_VdW_{,free}$ is LJ terms for ligand/protein interaction and LJ terms for ligand/water interaction, respectively. $E\_Coul_{bound}$ and $E\_Coul_{,free}$ is electrostatic terms for ligand/protein interaction and electrostatic terms for ligand/water interaction, respectively, default scaling factors $\alpha = 0.18$ and $\beta = 0.50$ was used.

## 4. Results and discussion

### 4.1. Pharmacophore model generation and validation

This study is aimed to screen an inhibitor for MMP-9 which plays a major role in rheumatoid arthritis, atherosclerosis, metastasis and cancer [67]. Ligand based drug designing approach is employed to identify the novel molecules against MMP-9. The MMP-9 inhibitors and their activities ($IC_{50}$ values) used to generate the pharmacophore model were given in Supplementary Table S2. 89 ligands taken for this study include diazepine, hydroxamate and non-hydroxamate-type inhibitors, acyclic sulfonamide inhibitors, sulfonyl, 5-substituted 2-bisarylthiocyclopentane carboxylic acid.

Active and inactive threshold of $pIC_{50}$ of 8.00 and 5.42 were applied for the dataset to yield 24 actives, 14 inactive and 51 moderately actives. Only the active compounds are considered when developing common pharmacophore hypotheses. Using tree based partition algorithm with maximum tree depth of five, 14 five featured hypotheses from the variant list were generated. These pharmacophore hypotheses were selected and subjected to stringent scoring function analysis. Finally, Score hypotheses rank the above generated hypotheses by aligning to the active ligands. A summary of statistical data of best 3 common pharmacophore with survival score is listed in Table 1.

Pharmacophore hypothesis named AAARR.1813 has the best survival score of 3.707. The pharmacophore features present in this hypothesis have three hydrogen bond acceptors, and two ring aromatic regions which are shown in Fig. 2. The distances and angles of AAARR.1813 among the pharmacophore features are shown in Tables 2 and 3. The quality of pharmacophore was measured

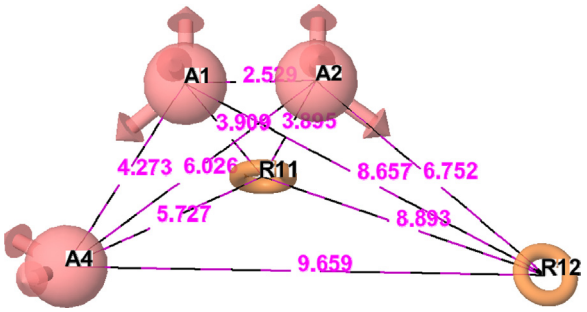


**Fig. 2.** The best generated pharmacophore model AAARR.1813, developed using Phase module. Pharmacophore features illustrating are hydrogen bond acceptor (A1, A2 and A4 pink), aromatic ring (R11 and R12 orange), with distances (in Å) between different sites. (For interpretation of the references to color in this figure legend, the reader is referred to the web version of the article.)

using the fitness and GH scoring functions. Fitness scores for all ligands were observed on the best scored pharmacophore model AAARR.1813 to check whether the hypotheses map well with highly active or inactive molecules. The hypotheses AAARR.1813 was well mapped with the active molecule (22), indicated that all the features were perfectly mapped and had a fitness score of 3.00 (Fig. 3) whereas least active molecule (**1**) was mapped with the only 3 features and had a fitness score of 1.68 shown in Fig. 3. This indicates that generated pharmacophore model AAARR.1813 was able to pick the active novel molecules rather inactives from the database.

The quality of AAARR.1813 was also validated using GH scoring method. The results were analyzed using the hit list (Ht), number of active percent of yields (%*Y*), percent ratio of actives in the hit list (%*A*), enrichment factor (*E*), false negatives, false positives and goodness of hit score. The hypotheses AAARR.1813 was successful in retrieving 95% of active compounds from the decoys set (Table 4). In addition, the calculated EF and GH score for ligand based pharmacophore model are found to be 28.72, 0.659 indicates that quality of the pharmacophore model is acceptable [68]. This study suggests that the hypothesis is good in discriminating the actives from inactives and retrieves the active inhibitors of MMP-9.

### 4.2. Pharmacophore screening

The best hypothesis AAARR.1813 was used as a 3D query for retrieving the active molecules from Duke's database using Phase software [69]. The virtual screening of Dukes database (http://www.ars-grin.gov/duke/) has yielded five molecules by matching the predicted hypotheses (AAARR.1813) to the ligand sites of the duke's database and ranks the molecules based on the

**Table 2**
Distances between the different pharmacophoric features of AAARR.1813 hypothesis.

| Site1 | Site2 | Distance |
|---|---|---|
| A2 | A1 | 2.529 |
| A2 | A4 | 6.026 |
| A2 | R11 | 3.895 |
| A2 | R12 | 6.752 |
| A1 | A4 | 4.273 |
| A1 | R11 | 3.909 |
| A1 | R12 | 8.657 |
| A4 | R11 | 5.727 |
| A4 | R12 | 9.659 |
| R11 | R12 | 8.893 |

**Table 3**
Angles between the different pharmacophoric features of AAARR.1813 hypothesis.

| Site1 | Site2 | Site3 | Angle | Site1 | Site2 | Site3 | Angle |
|---|---|---|---|---|---|---|---|
| A1 | A2 | A4 | 36.7 | A1 | A4 | R11 | 43 |
| A1 | A2 | R11 | 71.4 | A1 | A4 | R12 | 63.7 |
| A1 | A2 | R12 | 132.2 | R11 | A4 | R12 | 64.9 |
| A4 | A2 | R11 | 66.5 | A2 | R11 | A1 | 37.8 |
| A4 | A2 | R12 | 98 | A2 | R11 | A4 | 74.9 |
| R11 | A2 | R12 | 110.4 | A2 | R11 | R12 | 45.4 |
| A2 | A1 | A4 | 122.6 | A1 | R11 | A4 | 48.2 |
| A2 | A1 | R11 | 70.8 | A1 | R11 | R12 | 73.8 |
| A2 | A1 | R12 | 35.3 | A4 | R11 | R12 | 79.5 |
| A4 | A1 | R11 | 88.7 | A2 | R12 | A1 | 12.5 |
| A4 | A1 | R12 | 90.1 | A2 | R12 | A4 | 38.2 |
| R11 | A1 | R12 | 80.5 | A2 | R12 | R11 | 24.2 |
| A2 | A4 | A1 | 20.7 | A1 | R12 | A4 | 26.3 |
| A2 | A4 | R11 | 38.6 | A1 | R12 | R11 | 25.7 |
| A2 | A4 | R12 | 43.8 | A4 | R12 | R11 | 35.7 |

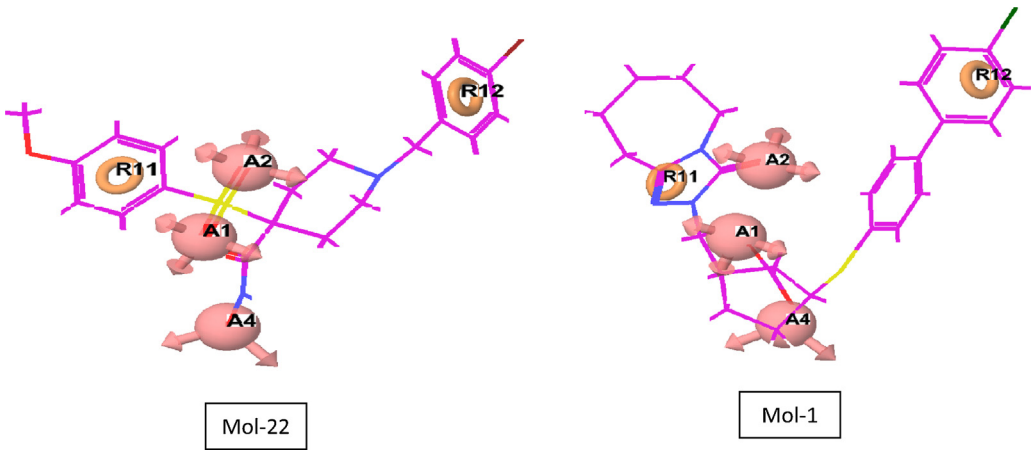


**Fig. 3.** Pharmacophore mapping of the active (22) and least active (1) compound on the best pharmacophore model AAARR.1813.

**Table 4**
Ligand based pharmacophore model evaluation using Güner-Henry scoring method for MMP-9.

| | |
|---|---|
| Total number of molecules in the database (D) | 2548 |
| Total number of actives in the database (A) | 48 |
| Total Hits (Ht) | 85 |
| Active Hits (Ha) | 46 |
| %Yield of actives [(Ha/Ht) * 100)] | 54.11 |
| %Ratio of actives [(Ha/*A*) * 100)] | 95.33 |
| Enrichment factor (E) (Ha * *D*)/(Ht * *A*) | 28.72 |
| False negatives (*A*–Ha) | 2 |
| False positives (Ht–Ha) | 39 |
| Goodness of hit score[a] | 0.659 |

%*A* is the percentage of known active compounds obtained from the database, Ha is the number of actives in the hits list (true positives), *A* is the number of active compounds in the database, %*Y* is the percentage of known actives in the hits list (recall), Ht is the number of hits retrieved, *D* is the number of compounds in the database, *E* is the enrichment of the concentration of actives by the model relative to random screening without a pharmacophoric approach, and GH is the Güner-Henry score. GH score of 0.6 – 1 indicates a very good model.

[a] $[(Ha(3At + Ht)/4HtA)) \times (1 - ((Ht - Ha)/(D - A))]$.

fitness score. The fitness scores and matched ligand sites for the above 5 molecules were listed (Table 5). Apart from 5 molecules, the known highly active from the dataset were taken to compare the binding modes with the receptor MMP-9.

### 4.3. Docking validation

In this work docking validation was performed by redocking co-crystallized ligand NFH into their respective binding sites. We found that the redocked NFH reproduced the binding pose of the co-crystal ligand with the glide score of −8.37 kcal/mol. The RMS deviation for the docked and experimental pose was analyzed. The RMSD for both the ligands was 0.18 Å, indicating that the docking program was successful in reproducing the native pose. Hence this program was further used to identify the binding pose of the novel hits. Fig. 4 shows the alignment of redocked (pink) and co crystal ligand (green).

**Table 5**
Fitness scores and matched ligand sites for the ligand based hits.

| Entry ID | Title | Matched ligand sites | Fitness |
|---|---|---|---|
| 1 | Known ligand | A(2) A(1) A(4) R(11) R(12) | 3.00 |
| 1 | 5281627(Hinokiflavone) | A(6) A(5) A(7) R(16) R(17) | 1.28 |
| 2 | 330034(Arctiin) | A(11) A(8) A(2) R(20) R(21) | 1.16 |
| 3 | 5358042 (Amphibine E) | A(3) A(1) A(5) R(16) R(17) | 0.72 |
| 4 | 5358035 (Amphibine C) | A(3) A(1) A(4) R(14) R(15) | 0.35 |
| 5 | 5318120 (Amphibine D) | A(1) A(3) A(5) R(14) R(15) | 0.12 |

### 4.4. Docking of ligands to MMP-9

XP ligand docking was performed for the 6 ligand molecules using the Glide module from the Maestro package. The best compounds were selected based on the glide score and its interaction with amino acid residues of S1′ loop (pocket). Interestingly known active ligand was found to have lesser docking score compared to novel natural compounds. Here the binding modes of the known and 2 identified compounds from natural compound database are described below. It can be seen from the screening results that the glide scores (Table 6) for the compounds **4**–**6** were less, hence these compounds were not considered for further analysis.

### 4.5. Binding mode of highly active known ligand

The known ligand diazepine binds into a deep catalytic active site which is formed by the hinge region (residues 420–431) through five hydrogen bonds. The hydroxyl group (O6, H15) forms hydrogen bonds with the amino group of Glu 427 with a distance of 3.18 Å, while Arg 424 (NH1) forms hydrogen bonds with the oxygen group of ligand (O4) (CO–NH) with a distance of 2.79 Å. The oxygen of sulfonyl group (O1) is in hydrogen bonding distance with the $NH_2$ and $NH_1$ group of Arg 424 with a distance of 3.23 Å and 2.67 Å respectively and also forms a hydrogen bond with the OH group of

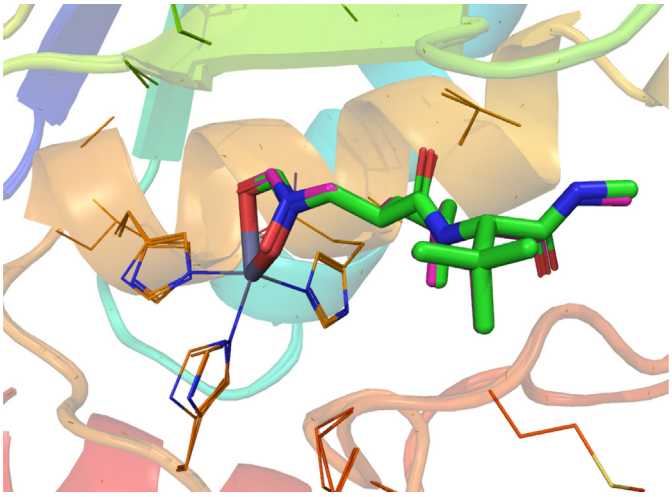

**Fig. 4.** shows the alignment of redocked (pink) and co crystal ligand (green) in the active site of MMP-9. (For interpretation of the references to color in this figure legend, the reader is referred to the web version of the article.)

**Table 6**
Glide docking XP score, energies, Vander waalscore and Xp H-bond and fitness scores for ligand based hits.

| S. no ligand | Glide score (kcal/mol) | Glide energy | Glide evdw | XpHBond | Fitness |
|---|---|---|---|---|---|
| 1. 5281627(Hinokiflavone) | −8.541 | −51.694 | −41.850 | −1.909 | 1.28 |
| 2. 330034 (Arctiin) | −8.505 | −50.344 | −41.945 | −2.299 | 1.16 |
| 3. Known ligand(diazepine) | −6.655 | −38.588 | −37.774 | −0.894 | 1.35 |
| 4. 5358042 (Amphibine E) | −5.289 | −33.289 | −32.513 | −1.494 | 0.72 |
| 5. 5358035 (Amphibine C) | −5.177 | −29.183 | −22.935 | −1.445 | 0.35 |
| 6. 5318120 (Amphibine D) | −4.852 | −37.332 | −30.799 | −0.620 | 0.12 |

Thr 426 with a distance of 2.80 Å. The LigPlus package [70] was used to show the interactions, which demonstrates that the hydrophobic interaction predominantly seen with amino acid residues in S1′ pocket such as Pro 415, Glu 416, Arg 424, Thr 426, Glu 427, Gly 428, Pro 429, Leu 431 and Lys 433 (Fig. 5(a)).

### 4.6. Docking of natural compounds with MMP-9

#### 4.6.1. Hinokiflavone from Juniperus communis (PubChem id: 5281627) (Model-1)

The compound hinokiflavone binds into a deep catalytic active site formed by the hinge region (residues 420–431) through three hydrogen bonds, similar to that of the known ligand. The hydroxyl group of benzene ring (O10, H18) forms hydrogen bonds with the NH group of Gly 215 (distance 3.13 Å). The amino group (NH) of Tyr 423 shares a hydrogen bond with the oxygen group (O3) of the ligand with a distance of 3.38 Å. The hydroxyl group of benzene ring (O5) forms hydrogen bonds with the CO group of Glu 402 (distance 2.57 Å). Furthermore, the ligand binds to the hydrophobic surface formed by S1′ pocket such as Gly 186, Leu 187, Leu 188, Ala 189, Lys 214, Gly 215, Tyr 393, Val 398, His 401, Glu 402, Pro 421, Met 422, Tyr 423 and Phe 425, which clearly explains the ability of this natural compound to bind to the MMP-9 S1 pocket. (Fig. 5(b)).

#### 4.6.2. Arctiin from arctiumlappa (PubChem id: 330034) (Model-2)

The compound Arctiin binds in a deep catalytic active site formed by the hinge region (residues 420–431) through three hydrogen bonds. The hydroxyl group (OH) of the ligand shares a hydrogen bond with the carboxyl group (CO) of Glu 402 with a distance of 2.88 Å and 3.16 Å. The backbone carboxyl group (C=O) of Pro 421 forms a hydrogen bond with the hydroxyl group (OH) of the ligand (distance of 3.08 Å). The hydrophobic surface formed by Gly 186, Leu 188, Ala 189, Gly 215, Tyr 393, Val 398, His 401, Pro 421, Met 422 and Tyr 423 stabilize the interaction (ligand protein complex) (Fig. 5(c)).

Comparison of the docking pose of known and searched compounds suggests that these compounds occupy the S1′ loop of MMP-9. The compounds hinokiflavone and Arctiin have a minimum of 2 H-bonds and hydrophobic interactions in the S1′ loop, suggesting that these compounds may possess activity against MMP-9 as similar to that of the known active ligand.

**Table 7**
Average RMSD of Model complex.

| RMSD (Å) | Model-1 | Model-2 |
|---|---|---|
| Protein | 1.92 | 1.83 |
| Ligand | 0.67 | 0.60 |

#### 4.6.3. Molecular dynamics simulation of Hinokiflavone and Arctiin

In order to compare the two active ligands Hinokiflavone (Model-1) and Arctiin (Model-2) in the binding process, molecular dynamics simulation of the bound complexes was undertaken. To explore the dynamical stability of both complexes, root mean square deviation from the starting structure was analyzed. The results are shown in Fig. 6. The plot shows that both the systems reach equilibrium within 2 ns. The average RMSD for the protein and the ligand for both models are shown in Table 7. The analysis of root mean square fluctuation (RMSF) of each residue for both models is presented in Fig. 7. The fluctuations of the residues are higher in model-2 than they are in model-1. The protein structures of the two systems share different trends of dynamic features due to the mode of binding of the respective ligands. The fluctuations of the residues in the S1 site are similar in both models. The visualization of the trajectory shows that both ligands are always anchored into the S1pocket throughout the dynamics simulation.

The important interaction between the protein–ligand complexes is the hydrogen bonding interaction which is listed in Table 8. It shows that Pro 421, Glu 402 and Phe 425 form a hydrogen bond with ligand in model-1, whereas in model-2, Glu 427 forms a hydrogen bond with the ligand. In both the models the ligand forms a stable H-bond with Glu 427.

#### 4.6.4. Binding free energy analysis

The binding affinities of both ligands with MMP-9 were calculated using Eq. (1). The results are shown in Table 8. It can be seen that there is a large difference of the calculated binding free energy for ligands hinokiflavone and arctiin, which corresponds to the difference in the binding affinity. The difference in $\Delta G_{binding}$ is estimated to be 9.13 kJ/mol for the ligands hinokiflavone and

**Table 8**
Hydrogen bond interaction between the ligand and the receptor from molecular dynamics trajectories and free energy of binding for the model systems.

| | Donor | Residue no | Atom | Acceptor residue | Residue no | Atom | Occupancy |
|---|---|---|---|---|---|---|---|
| Model-1 | Ligand | 165 | O5 | Glu | 402 | OE2 | 88.76 |
| | Ligand | 165 | O4 | Glu | 402 | OE2 | 67.52 |
| | Ligand | 165 | O6 | Pro | 421 | O | 61.46 |
| | Phe | 425 | N | Ligand | 165 | O10 | 31.79 |
| | Phe | 425 | N | Ligand | 165 | O11 | 30.1 |
| Model-2 | Ligand | 165 | O9 | ASP | 77 | OD1 | 91.48 |
| | Glu | 427 | N | Ligand | 165 | O6 | 69.99 |

| Energy (kJ/mol) | Model-1 | Model-2 |
|---|---|---|
| $\Delta G_{binding}$ | −26.54 | −17.40 |

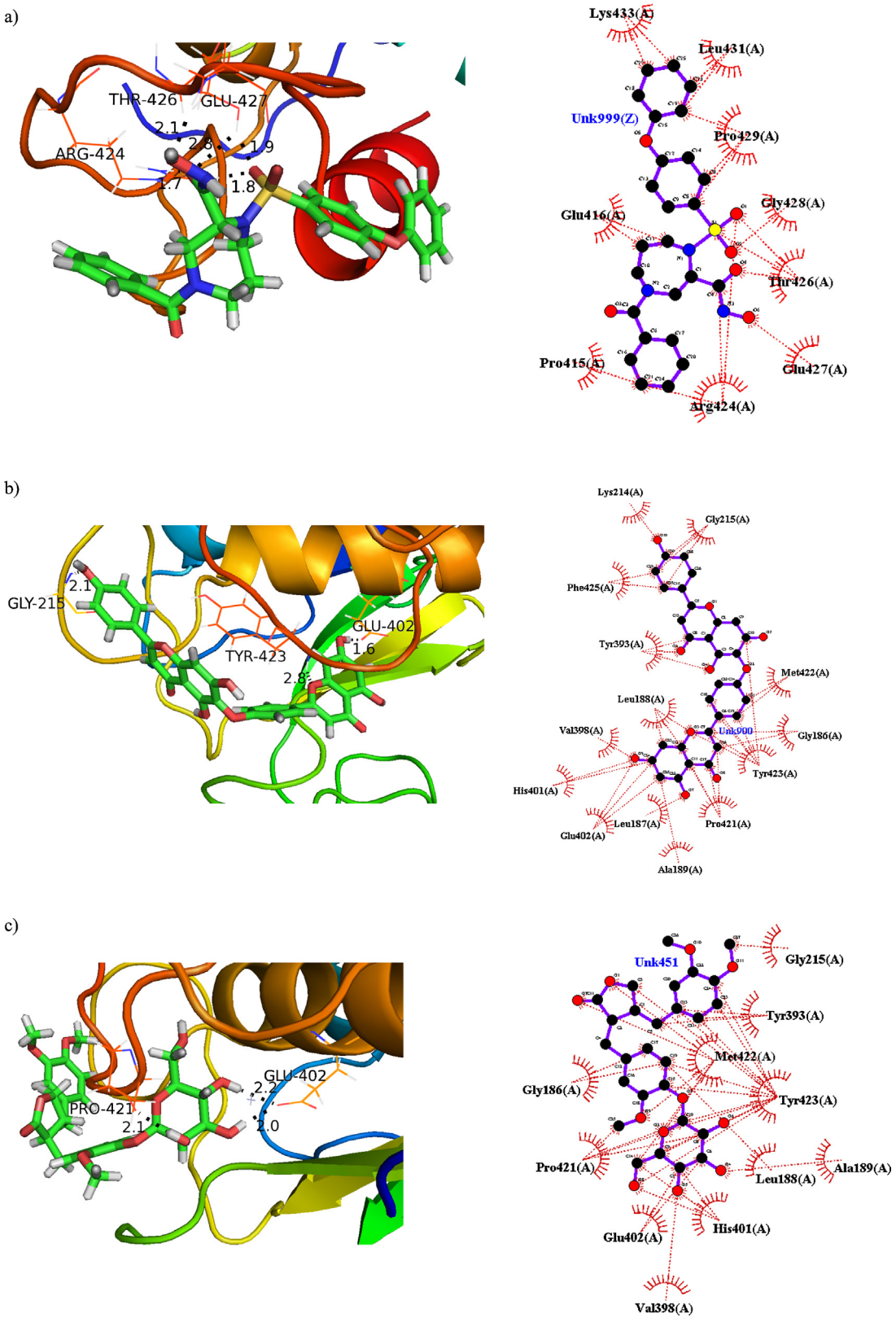


**Fig. 5.** Docking pose of (a) highly active ligand (diazepine) (b) 5281627 and (c) 330034 with S1 loop of MMP-9. H-bond is represented as dashed line and spiked residue represents hydrophobic contacts which were analyzed using LigPlus.

arctiin. Previous research suggests that highest binding free energy is crucial parameter in determining the selectivity, charge complementarity and packing with the MMP receptors [71]. Binding free energies of model-1 (Hinokiflavone) is in good agreement with that of the previous studies on the natural compound inhibitors like quercetin and astaxanthin [72,73]. The above ligands show comparable free energy of binding to MMP-9, which would provide new insight for the design of inhibitors for MMP-9 with high specificity

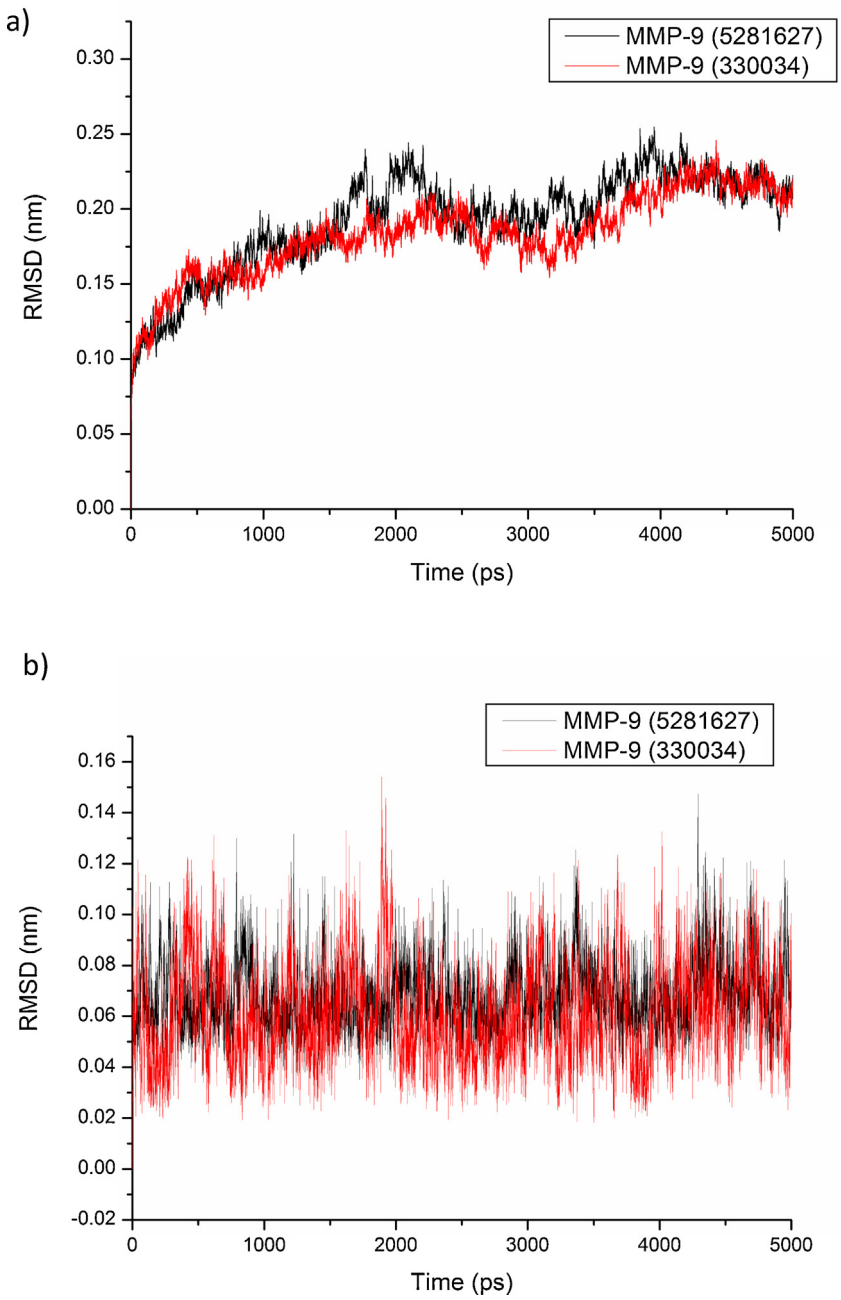


**Fig. 6.** RMSD of the (a) protein and (b) ligand with respect to time for Model-1 and Model-2.

[71,74,75]. Steered molecular dynamics (SMD) simulation has been used to compare the binding affinity of Hinokiflavone and Arctiin based on the hypothesis that the larger the force needed to unbind a ligand binding, the greater the affinity. Force required to unbind Hinokiflavone and Arctiin is shown in Fig. 8. From the figure it can be clearly seen that the unbinding of Hinokiflavone from the active site of MMP-9 requires higher force when compared to Arctiin, which is in arrangement with the binding free energy. Hence, Hinokiflavone was used in the current research for further experimental studies.

### 4.7. Cell viability (MTT) assay

The top ranked compound Hinokiflavone was purchased from Mol port (CAS 19202-36-9) for further in vitro analysis. The cytotoxic effect of hinokiflavone on proliferation of MCF-7 cell line was assessed using MTT method. Comparing the results of the control group of untreated cells with treated cells, treated cells exhibited a dose dependent decline in viability, the highest viability was 96.3% and the lowest was 49% after 48 h incubation. In terms of cytotoxicity index, the compound with 1.857 mM showed 50% cytotoxicity. Hence, the $LC_{50}$ was determined as 1.857 mM.

### 4.8. Gelatin zymography

Matrix metalloproteinases (MMPs) released by tumor cells into the extracellular environment are crucial for cancer-promoted tissue degradation and invasion along with the metastatic process [76–78]. The inhibitory activity of hinokiflavone (1.857 mM) for MMP-9 was evaluated using MCF-7 breast cancer cell line. MMP-9 from the conditioned medium of MCF-7 culture was submitted to gelatin zymography and showed a decrease of MMP-9 activity (Fig. 9A). The gel on visual observation did show complete

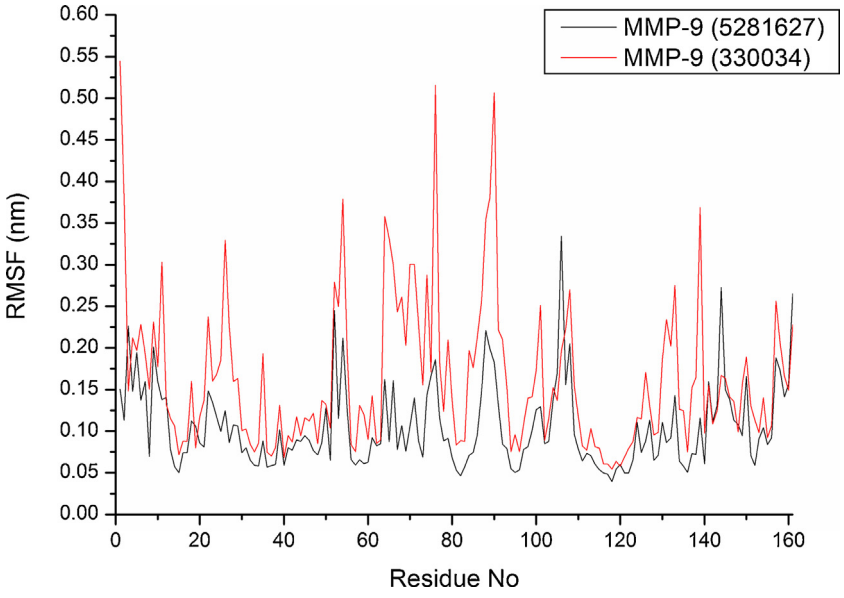


**Fig. 7.** RMSF of the protein for each residue for Model-1 and Model-2.

inhibition of MMP-9 in the presence of hinokiflavone, however the densitometric analysis showed a decreased MMP-9 activity compared to control (Fig. 9B).

Previous studies report that MMPs expression is correlated with cancer metastasis and that they play a vital role in the metastatic process [79]. The zymography results are in accordance with previous reports correlating MMP activity in cancer metastasis [80,81]. In the present study, we provide evidence that hinokiflavone is able to inhibit MMP-9 in vitro, suggesting that hinokiflavone might possess anti-metastatic potential.

### 4.9. Gelatinolytic assay for inhibition studies

The optical density values for the varying concentrations of gelatin (0.1–10 μg) were determined from 0.06 to 1.58, respectively. $R^2$ coefficient value of 0.984 was determined (Fig. 10A). As stated in the referred article, the increasing concentrations of gelatin after 10 μg showed a plateau effect (data not shown) which was taken as the total amount of gelatin substrate for the enzyme assay [65]. The CBB is known to strongly react with proteins. The presence of MMP-9 protein gave an enhanced color formation resulting in a false negative response. A substrate blank (SB) was analyzed to eliminate all background colors in the reaction. The inhibitory effect of hinokiflavone on the enzyme was expressed in percentage of the control and calculated using the formula $[(A_{600}\ \mathrm{EI} - A_{600}\ \mathrm{SB} - A_{600}\ B) - (A_{600}\ E0 - A_{600}\ \mathrm{SB} - A_{600}\ B)]/(A_{600}\ \mathrm{EB} - A_{600}\ B) \times 100$. Where, $A_{600}\ B$ is the absorbance value of control with only CBB R-250 and $ME_2SO$, $A_{600}$ EI is the absorbance value of the varying concentrations of the enzyme-inhibitor samples, $A_{600}$ E0 is the absorbance value of the enzyme sample without inhibitor, $A_{600}$ SB is the absorbance value of the control devoid of substrate and $A_{600}$ of EB is the absorbance value of the control devoid of enzyme. The increasing concentrations from 10 μM of Hinokiflavone inhibit the enzyme progressively and complete inhibition observed above

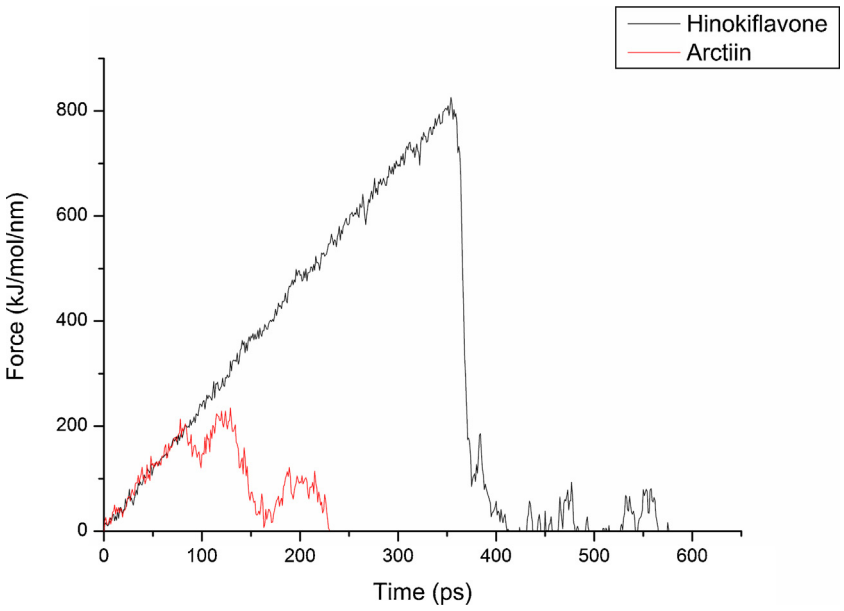


**Fig. 8.** Forced unbinding profile of Hinokiflavone and Arctiin.

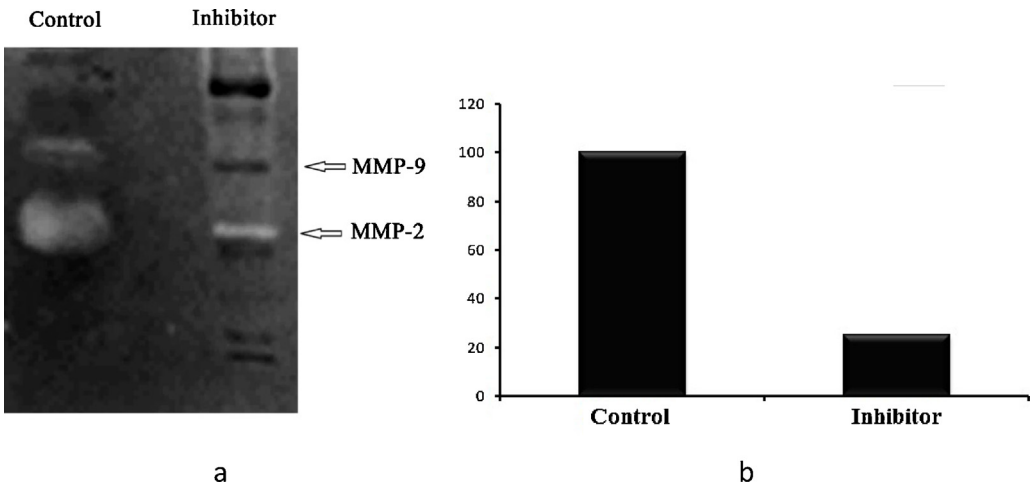


**Fig. 9.** (A) Gelatin zymography for the determination of MMP-2 and MMP-9 activities in MCF-7 cancer cell line. Increased MMP-2 and MMP-9 activities were evidenced (control) by the native PAGE analysis when compared to the inhibitor at concentration of (1.857 μM). (B) Densitometric analysis of MMP-9 activity.

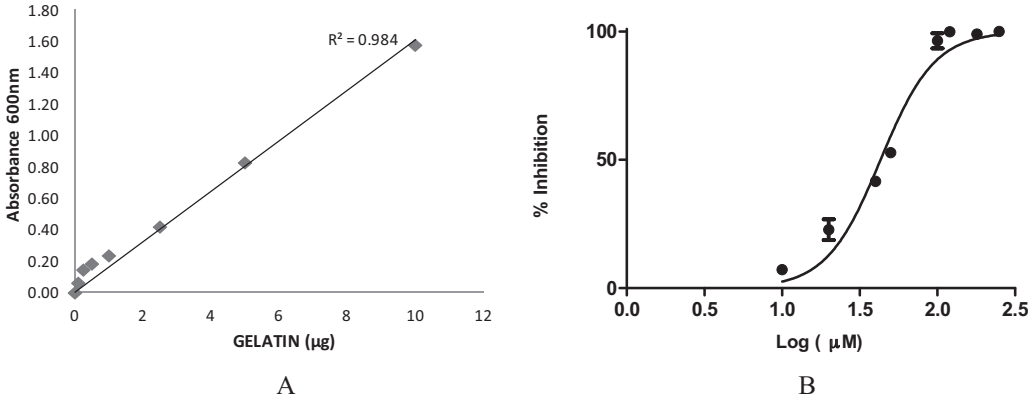


**Fig. 10.** (A) Standard plot for gelatin concentration quantification. Analyzed with CBB R-250 and read at 600 nm. All tests were done in triplicates. (B) The graph depicts the effect of Hinokiflavone (10–250 μM) expressed in log values on MMP9 activity. The values were averaged and expressed as percentage inhibition on the enzyme control (without Hinokiflavone). All tests were done in triplicate. Bars signify the standard deviation.

100 μM. The mean percentage inhibition for inhibitor concentrations of 10, 20, 40, 50 and 100 μM were 7.24, 22.82, 41.65, 52.91 and 96.55%, respectively. The graph was plotted with percentage enzyme inhibition versus inhibitor concentration expressed as log (μM). The $IC_{50}$ for hinokiflavone was calculated as 43.08 μM ($R^2$ = 0.96) (Fig. 10B).

## 5. Conclusions

Pharmacophore modeling for the MMP-9 inhibitors was performed and five featured pharmacophore hypotheses were developed. A five point pharmacophore with three hydrogen bond acceptors and two ring aromatic with high survival score were predicted. The developed ligand based pharmacophore model was validated using GH scoring method. The ligand based pharmacophore model was successful in retrieving the 95% of active compounds from the decoys set. This pharmacophore hypothesis is further used to screen the natural compound database for the identification of potential MMP-9 inhibitors. From in silico studies, a natural compound hinokiflavone was found to have a good glide score, binding free energy of −26.54 kJ/mol and stable interaction with S1 loop of MMP-9 when compared with the known synthetic compounds. The inhibitory action of the compound hinokiflavone was tested in vitro using zymography and Colorimetric Gelatinolytic methods. The $IC_{50}$ value on MMP-9 of the compound was 43.08 μM. We speculate that the inhibition of metastasis-specific MMP-9 in cancer cells could be one of the targets for anticancer function, and thus provides the molecular basis for the development of hinokiflavone as a novel agent for cancer metastasis.

## Acknowledgements

The authors wish to thank the Department of Biotechnology (DBT), New Delhi, India for Financial Support to Dr. V. Subramanian. Authors wish to thank Dr. A.B. Mandal, Director CLRI for their continued support. SK would like to acknowledge SRM University and his colleague S. Mukund for their constant support.

## Appendix A. Supplementary data

Supplementary material related to this article can be found, in the online version, at http://dx.doi.org/10.1016/j.jmgm.2013.12.008.

## References

[1] P. Vihinen, R. Ala-aho, V.M. Kahari, Matrix metalloproteinases as therapeutic targets in cancer, Current Cancer Drug Targets 5 (2005) 203–220.
[2] P. Vihinen, V.M. Kahari, Matrix metalloproteinases in cancer: prognostic markers and therapeutic targets, International Journal of Cancer 99 (2002) 157–166.
[3] N. Johansson, M. Ahonen, V.M. Kahari, Matrix metalloproteinases in tumor invasion, Cellular and Molecular Life Sciences 57 (2000) 5–15.

[4] V.M. Kahari, U. Saarialho-Kere, Matrix metalloproteinases and their inhibitors in tumour growth and invasion, Annals of Medicine 31 (1999) 34–45.
[5] R.P. Verma, C. Hansch, Matrix metalloproteinases (MMPs): chemical–biological functions and (Q)SARs, Bioorganic & Medicinal Chemistry 15 (2007) 2223–2268.
[6] O. Nicolotti, T.F. Miscioscia, F. Leonetti, G. Muncipinto, A. Carotti, Screening of matrix metalloproteinases available from the protein data bank: insights into biological functions, domain organization, and zinc binding groups, Journal of Chemical Information and Modeling 47 (2007) 2439–2448.
[7] F. Vasaturo, F. Solai, C. Malacrino, T. Nardo, B. Vincenzi, M. Modesti, et al., Plasma levels of matrix metalloproteinases 2 and 9 correlate with histological grade in breast cancer patients, Oncology Letters 5 (2013) 316–320.
[8] C. Chang, Z. Werb, The many faces of metalloproteases: cell growth, invasion, angiogenesis and metastasis, Trends in Cell Biology 11 (2001) S37–S43.
[9] N.I. Solovyeva, S.V. Vinokurova, O.S. Ryzhakova, T.A. Gureeva, I.V. Tsvetkova, Expression of gelatinases A and B and their endogenous regulators in immortal and transformed fibroblasts, Biomeditsinskaia khimiia 55 (2009) 441–450.
[10] H.Q. Ye, D.T. Azar, Expression of gelatinases A and B, and TIMPs 1 and 2 during corneal wound healing, Investigative Pphthalmology & Visual Science 39 (1998) 913–921.
[11] P.A. Forsyth, T.D. Laing, A.W. Gibson, N.B. Rewcastle, P. Brasher, G. Sutherland, et al., High levels of gelatinase-B and active gelatinase-A in metastatic glioblastoma, Journal of Neuro-Oncology 36 (1998) 21–29.
[12] J. Vandooren, P.E. Van den Steen, G. Opdenakker, Biochemistry and molecular biology of gelatinase B or matrix metalloproteinase-9 (MMP-9): the next decade, Critical Reviews in Biochemistry and Molecular Biology 48 (2013) 222–272.
[13] W.T. Purcell, M.A. Rudek, M. Hidalgo, Development of matrix metalloproteinase inhibitors in cancer therapy, Hematology/Oncology Clinics of North America 16 (2002) 227–1189.
[14] S. Rowsell, P. Hawtin, C.A. Minshull, H. Jepson, S.M. Brockbank, D.G. Barratt, et al., Crystal structure of human MMP9 in complex with a reverse hydroxamate inhibitor, Journal of Molecular Biology 319 (2002) 173–181.
[15] A. Tandon, S. Sinha, Structural insights into the binding of MMP9 inhibitors, Bioinformation 5 (2011) 310–314.
[16] T. Tuccinardi, E. Nuti, G. Ortore, A. Rossello, S.I. Avramova, A. Martinelli, Development of a receptor-based 3D-QSAR study for the analysis of MMP2, MMP3, and MMP9 inhibitors, Bioorganic & Medicinal Chemistry 16 (2008) 58–7749.
[17] B.G. Rao, Recent developments in the design of specific matrix metalloproteinase inhibitors aided by structural and computational studies, Current Pharmaceutical Design 11 (2005) 295–322.
[18] L. Devel, B. Czarny, F. Beau, D. Georgiadis, E. Stura, V. Dive, Third generation of matrix metalloprotease inhibitors: gain in selectivity by targeting the depth of the S1′ cavity, Biochimie 92 (2010) 8–1501.
[19] A. Agrawal, D. Romero-Perez, J.A. Jacobsen, F.J. Villarreal, S.M. Cohen, Zinc-binding groups modulate selective inhibition of MMPs, ChemMedChem 3 (2008) 812–820.
[20] F. Mannello, G. Tonti, S. Papa, Matrix metalloproteinase inhibitors as anticancer therapeutics, Current Cancer Drug Targets 5 (2005) 285–298.
[21] N.G. Lia, Z.H. Shib, Y.P. Tang, J.A. Duan, Selective matrix metalloproteinase inhibitors for cancer, Current Medicinal Chemistry 16 (2009) 27–3805.
[22] B. Turk, Targeting proteases: successes, failures and future prospects, Nature Reviews Drug Discovery 5 (2006) 785–799.
[23] L. Devel, V. Rogakos, A. David, A. Makaritis, F. Beau, P. Cuniasse, et al., Development of selective inhibitors and substrate of matrix metalloproteinase-12, Journal of Biological Chemistry 281 (2006) 11152–11160.
[24] L.A. Reiter, K.D. Freeman-Cook, C.S. Jones, G.J. Martinelli, A.S. Antipas, M.A. Berliner, et al., Potent, selective pyrimidinetrione-based inhibitors of MMP-13, Bioorganic & Medicinal Chemistry Letters 16 (2006) 5822–5826.
[25] K. Maeda, M. Kuzuya, X.W. Cheng, T. Asai, S. Kanda, N. Tamaya-Mori, et al., Green tea catechins inhibit the cultured smooth muscle cell invasion through the basement barrier, Atherosclerosis 166 (2003) 23–30.
[26] F. Mannello, Natural bio-drugs as matrix metalloproteinase inhibitors: new perspectives on the horizon? Recent Patents on Anti-Cancer Drug Discovery 1 (2006) 91–103.
[27] S. Kalva, S. Vadivelan, R. Sanam, S.A. Jagarlapudi, L.M. Saleena, Lead identification and optimization of novel collagenase inhibitors; pharmacophore and structure based studies, Bioinformation 8 (2012) 301.
[28] T. Le Diguarher, A.M. Chollet, M. Bertrand, P. Hennig, E. Raimbaud, M. Sabatini, et al., Stereospecific synthesis of 5-substituted 2-bisarylthiocyclopentane carboxylic acids as specific matrix metalloproteinase inhibitors, Journal of Medicinal Chemistry 46 (2003) 52–3840.
[29] C.A. Fink, J.E. Carlson, C. Boehm, P. McTaggart, Y. Qiao, J. Doughty, et al., Design and synthesis of thiol containing inhibitors of matrix metalloproteinases, Bioorganic & Medicinal Chemistry Letters 9 (1999) 195–200.
[30] V. Aranapakam, J.M. Davis, G.T. Grosu, J. Baker, J. Ellingboe, A. Zask, et al., Synthesis and structure-activity relationship of N-substituted 4-arylsulfonylpiperidine-4-hydroxamic acids as novel, orally active matrix metalloproteinase inhibitors for the treatment of osteoarthritis, Journal of Medicinal Chemistry 46 (2003) 2376–2396.
[31] J.I. Levin, J.M. Chen, K. Cheung, D. Cole, C. Crago, E.D. Santos, et al., Acetylenic TACE inhibitors Part 1. SAR of the acyclic sulfonamide hydroxamates, Bioorganic & Medicinal Chemistry Letters 13 (2003) 2799–2803.
[32] A.M. Venkatesan, J.M. Davis, G.T. Grosu, J. Baker, A. Zask, J.I. Levin, et al., Synthesis and structure-activity relationships of 4-alkynyloxy phenyl sulfanyl, sulfinyl, and sulfonyl alkyl hydroxamates as tumor necrosis factor-alpha converting enzyme and matrix metalloproteinase inhibitors, Journal of Medicinal Chemistry 47 (2004) 6255–6269.
[33] S. Hanessian, S. Bouzbouz, A. Boudon, G.C. Tucker, D. Peyroulan, Picking the S1, S1′ and S2′ pockets of matrix metalloproteinases. A niche for potent acyclic sulfonamide inhibitors, Bioorganic & Medicinal Chemistry Letters 9 (1999) 1691–1696.
[34] J.I. Levin, J.F. DiJoseph, L.M. Killar, A. Sung, T. Walter, M.A. Sharr, et al., The synthesis and biological activity of a novel series of diazepine MMP inhibitors, Bioorganic & Medicinal Chemistry Letters 8 (1998) 2657–2662.
[35] H.J. Breyholz, M. Schafers, S. Wagner, C. Holtke, A. Faust, H. Rabeneck, et al., C-5-disubstituted barbiturates as potential molecular probes for noninvasive matrix metalloproteinase imaging, Journal of Medicinal Chemistry 48 (2005) 3400–3409.
[36] V. Aranapakam, G.T. Grosu, J.M. Davis, B. Hu, J. Ellingboe, J.L. Baker, et al., Synthesis and structure–activity relationship of alpha-sulfonylhydroxamic acids as novel, orally active matrix metalloproteinase inhibitors for the treatment of osteoarthritis, Journal of Medicinal Chemistry 46 (2003) 2361–2375.
[37] D.J. Osguthorpe, W. Sherman, A.T. Hagler, Generation of receptor structural ensembles for virtual screening using binding site shape analysis and clustering, Chemical Biology & Drug Design 80 (2012) 182–193.
[38] S.L. Dixon, A.M. Smondyrev, E.H. Knoll, S.N. Rao, D.E. Shaw, R.A. Friesner, PHASE: a new engine for pharmacophore perception 3D QSAR model development, and 3D database screening: 1. Methodology and preliminary results, Journal of Computer-Aided Molecular Design 20 (2006) 647–671.
[39] P.R. Murumkar, V.P. Zambre, M.R. Yadav, Development of predictive pharmacophore model for in silico screening, and 3D QSAR CoMFA and CoMSIA studies for lead optimization, for designing of potent tumor necrosis factor alpha converting enzyme inhibitors, Journal of Computer-Aided Molecular Design 24 (2010) 143–156.
[40] W. Tai, T. Lu, H. Yuan, F. Wang, H. Liu, S. Lu, et al., Pharmacophore modeling and virtual screening studies to identify new c-Met inhibitors, Journal of Molecular Modeling 18 (2012) 3087–3100.
[41] T.B. Lowinger, B. Riedl, J. Dumas, R.A. Smith, Design and discovery of small molecules targeting raf-1 kinase, Current Pharmaceutical Design 8 (2002) 2269–2278.
[42] R.A. Smith, J. Barbosa, C.L. Blum, M.A. Bobko, Y.V. Caringal, R. Dally, et al., Discovery of heterocyclic ureas as a new class of raf kinase inhibitors: identification of a second generation lead by a combinatorial chemistry approach, Bioorganic & Medicinal Chemistry Letters 11 (2001) 2775–2778.
[43] R.A. Friesner, R.B. Murphy, M.P. Repasky, L.L. Frye, J.R. Greenwood, T.A. Halgren, et al., Extra precision glide: docking and scoring incorporating a model of hydrophobic enclosure for protein–ligand complexes, Journal of Medicinal Chemistry 49 (2006) 6177–6196.
[44] M.J.G.W.T. Frisch, H.B. Schlegel, G.E. Scuseria, M.A. Robb, J.R. Cheeseman, J.A. Montgomery Jr., T. Vreven, K.N. Kudin, J.C. Burant, J.M. Millam, S.S. Iyengar, J. Tomasi, V. Barone, B. Mennucci, M. Cossi, G. Scalmani, N. Rega, G.A. Petersson, H. Nakatsuji, M. Hada, M. Ehara, K. Toyota, R. Fukuda, J. Hasegawa, M. Ishida, T. Nakajima, Y. Honda, O. Kitao, H. Nakai, M. Klene, X. Li, J.E. Knox, H.P. Hratchian, J.B. Cross, C. Adamo, J. Jaramillo, R. Gomperts, R.E. Stratmann, O. Yazyev, A.J. Austin, R. Cammi, C. Pomelli, J.W. Ochterski, P.Y. Ayala, K. Morokuma, G.A. Voth, P. Salvador, J.J. Dannenberg, V.G. Zakrzewski, S. Dapprich, A.D. Daniels, M.C. Strain, O. Farkas, D.K. Malick, A.D. Rabuck, K. Raghavachari, J.B. Foresman, J.V. Ortiz, Q. Cui, A.G. Baboul, S. Clifford, J. Cioslowski, B.B. Stefanov, G. Liu, A. Liashenko, P. Piskorz, I. Komaromi, R.L. Martin, D.J. Fox, T. Keith, M.A. Al-Laham, C.Y. Peng, A. Nanayakkara, M. Challacombe, P.M.W. Gill, B. Johnson, W. Chen, M.W. Wong, C. Gonzalez, J.A. Pople, Gaussian 03, Revision A.1, Gaussian, Inc., Pittsburgh PA, 2003.
[45] J.O. De Kerpel, U. Ryde, Protein strain in blue copper proteins studied by free energy perturbations, Proteins 36 (1999) 157–174.
[46] F. Lin, R. Wang, Systematic derivation of AMBER force field parameters applicable to zinc-containing systems, Journal of Chemical Theory and Computation 6 (2010) 1852–1870.
[47] M.B. Peters, Y. Yang, B. Wang, L. Fusti-Molnar, M.N. Weaver, K.M. Merz Jr., Structural survey of zinc containing proteins and the development of the zinc AMBER force field (ZAFF), Journal of Chemical Theory and Computation 6 (2010) 2935–2947.
[48] V. Rajapandian, V. Hakkim, V. Subramanian, Molecular dynamics studies on native, loop-contracted, and metal ion-substituted azurins, Journal of Physical Chemistry B 114 (2010) 8474–8486.
[49] U. Ryde, M.H. Olsson, B.O. Roos, A.C. Borin, A theoretical study of the copper–cysteine bond in blue copper proteins, Theoretical Chemistry Accounts 105 (2001) 452–462.
[50] E.I. Solomon, R.K. Szilagyi, S. DeBeer George, L. Basumallick, Electronic structures of metal sites in proteins and models: contributions to function in blue copper proteins, Chemical Reviews 104 (2004) 419–458.
[51] C. Dennison, Investigating the structure and function of cupredoxins, Coordination Chemistry Reviews 249 (2005) 3025–3054.
[52] P. Comba, M. Kerscher, Computation of structures and properties of transition metal compounds, Coordination Chemistry Reviews 253 (2009) 564–574.
[53] S. Shaik, S. Cohen, Y. Wang, H. Chen, D. Kumar, W. Thiel, P450 enzymes: their structure, reactivity, and selectivity-modeled by QM/MM calculations, Chemical Reviews 110 (2010) 949–1017.
[54] P.E. Siegbahn, M.R. Blomberg, Quantum chemical studies of proton-coupled electron transfer in metalloenzymes, Chemical Reviews 110 (2010) 7040–7061.

[55] K. Shahrokh, A. Orendt, G.S. Yost, T.E.3rd. Cheatham, Quantum mechanically derived AMBER-compatible heme parameters for various states of the cytochrome P450 catalytic cycle, Journal of Computational Chemistry 33 (2012) 119–133.
[56] D.A. Case, T.E.3rd Cheatham, T. Darden, H. Gohlke, R. Luo, K.M. Merz Jr., et al., The Amber biomolecular simulation programs, Journal of Computational Chemistry 26 (2005) 1668–1688.
[57] T. Makarewicz, R. Kazmierkiewicz, Molecular Dynamics Simulation by GROMACS Using GUI Plugin for PyMOL, Journal of Chemical Information and Modeling 53 (2013) 1229–1234.
[58] B. Hess, H. Bekker, H.J. Berendsen, J.G. Fraaije, LINCS: a linear constraint solver for molecular simulations, Journal of Computational Chemistry 18 (1997) 1463–1472.
[59] W. Li, H. Liu, E.E. Scott, F. Gräter, J.R. Halpert, X. Luo, et al., Possible pathway (s) of testosterone egress from the active site of cytochrome P450 2B1: a steered molecular dynamics simulation, Drug Metabolism and Disposition 33 (2005) 910–919.
[60] D.C. Marks, L. Belov, M.W. Davey, R.A. Davey, A.D. Kidman, The MTT cell viability assay for cytotoxicity testing in multidrug-resistant human leukemic cells, Leukemia Research 16 (1992) 1165–1173.
[61] D.T. Vistica, P. Skehan, D. Scudiero, A. Monks, A. Pittman, M.R. Boyd, Tetrazolium-based assays for cellular viability: a critical examination of selected parameters affecting formazan production, Cancer Research 51 (1991) 2515–2520.
[62] H. Takeuchi, M. Baba, S. Shigeta, An application of tetrazolium (MTT) colorimetric assay for the screening of anti-herpes simplex virus compounds, Journal of Virological Methods 33 (1991) 61–71.
[63] O.H. Lowry, N.J. Rosebrough, A.L. Farr, R.J. Randall, Protein measurement with the folin phenol reagent, Journal of Biological Chemistry 193 (1951) 265–275.
[64] K. Kupai, G. Szucs, S. Cseh, I. Hajdu, C. Csonka, T. Csont, et al., Matrix metalloproteinase activity assays: importance of zymography, Journal of Pharmacological and Toxicological Methods 61 (2010) 205–209.
[65] M. Osathanunkul, K. Buddhachat, S. Chomdej, A modified colorimetric method of gelatinolytic assay using bacterial collagenase, type II as a model, Analytical Biochemistry 433 (2013) 168–170.
[66] O.D. Defawe, R.D. Kenagy, C. Choi, S.Y. Wan, C. Deroanne, B. Nusgens, et al., MMP-9 regulates both positively and negatively collagen gel contraction A non-proteolytic function of MMP-9, Cardiovascular Research 66 (2005) 402–409.
[67] G.V. Halade, Y.F. Jin, M.L. Lindsey, Matrix metalloproteinase (MMP)-9: a proximal biomarker for cardiac remodeling and a distal biomarker for inflammation, Pharmacology & Therapeutics 139 (2013) 32–40.
[68] S. Thangapandian, S. John, S. Sakkiah, K.W. Lee, Ligand and structure based pharmacophore modeling to facilitate novel histone deacetylase 8 inhibitor design, European Journal of Medicinal Chemistry 45 (2010) 4409–4417.
[69] S.L. Dixon, A.M. Smondyrev, E.H. Knoll, S.N. Rao, D.E. Shaw, R.A. Friesner, PHASE: a new engine for pharmacophore perception, 3D QSAR model development, and 3D database screening: 1. Methodology and preliminary results, Journal of Computer-Aided Molecular Design 20 (2006) 647–671.
[70] R.A. Laskowski, M.B. Swindells, LigPlot+: multiple ligand–protein interaction diagrams for drug discovery, Journal of Chemical Information and Modeling 51 (2011) 2778–2786.
[71] R.C. Rizzo, S. Toba, I.D. Kuntz, A molecular basis for the selectivity of thiadiazole urea inhibitors with stromelysin-1 and gelatinase-A from generalized born molecular dynamics simulations, Journal of Medicinal Chemistry 47 (2004) 3065–3074.
[72] A.C. Saragusti, M.G. Ortega, J.L. Cabrera, D.A. Estrin, M.A. Marti, G.A. Chiabrando, Inhibitory effect of quercetin on matrix metalloproteinase 9 activity molecular mechanism and structure–activity relationship of the flavonoid–enzyme interaction, European Journal of Pharmacology 644 (2010) 138–145.
[73] Z. Bikadi, E. Hazai, F. Zsila, S.F. Lockwood, Molecular modeling of non-covalent binding of homochiral (3S,3′S)-astaxanthin to matrix metalloproteinase-13 (MMP-13), Bioorganic & Medicinal Chemistry 14 (2006) 5451–5458.
[74] T. Hou, W. Zhang, X. Xu, Binding affinities for a series of selective inhibitors of gelatinase-A using molecular dynamics with a linear interaction energy approach, Journal of Physical Chemistry B 105 (2001) 5304–5315.
[75] N. Carrascal, R.C. Rizzo, Calculation of binding free energies for non-zinc chelating pyrimidine dicarboxamide inhibitors with MMP-13, Bioorganic & Medicinal Chemistry Letters 19 (2009) 47–50.
[76] L.A. Liotta, K. Tryggvason, S. Garbisa, I. Hart, C.M. Foltz, S. Shafie, Metastatic potential correlates with enzymatic degradation of basement membrane collagen, Nature 284 (1980) 67–68.
[77] E.J. Bernhard, S.B. Gruber, R.J. Muschel, Direct evidence linking expression of matrix metalloproteinase 9 (92-kDa gelatinase/collagenase) to the metastatic phenotype in transformed rat embryo cells, Proceedings of the National Academy of Sciences of the United States of America 91 (1994) 4293–4297.
[78] Y. Tsunezuka, H. Kinoh, T. Takino, Y. Watanabe, Y. Okada, A. Shinagawa, et al., Expression of membrane-type matrix metalloproteinase 1 (MT1-MMP) in tumor cells enhances pulmonary metastasis in an experimental metastasis assay, Cancer Research 56 (1996) 5678–5683.
[79] M. Egeblad, Z. Werb, New functions for the matrix metalloproteinases in cancer progression, Nature Reviews. Cancer 2 (2002) 161–174.
[80] G. La Rocca, I. Pucci-Minafra, A. Marrazzo, P. Taormina, S. Minafra, Zymographic detection and clinical correlations of MMP-2 and MMP-9 in breast cancer sera, British Journal of Cancer 90 (2004) 1414–1421.
[81] X.M. Zhang, S.P. Huang, Q. Xu, Quercetin inhibits the invasion of murine melanoma B16-BL6 cells by decreasing pro-MMP-9 via the PKC pathway, Cancer Chemotherapy and Pharmacology 53 (2004) 82–88.